



**HAL**  
open science

## **A wide-spectrum 550-1600 nm, 16k VIS + 8 NIR pixels, high-dynamic range image-sensor for biomedical applications**

Laurent Alacoque, David Coriat, Jean-Michel Tualle, Valentin Espinas, Xavier Alacoque, Anabela da Silva, Guillaume Moritz, Sylvain Dumas, Dominique Etti

### **► To cite this version:**

Laurent Alacoque, David Coriat, Jean-Michel Tualle, Valentin Espinas, Xavier Alacoque, et al.. A wide-spectrum 550-1600 nm, 16k VIS + 8 NIR pixels, high-dynamic range image-sensor for biomedical applications. ICECS 2023 - 30th IEEE International Conference on Electronics, Circuits and Systems, IEEE, Dec 2023, Istanbul, Turkey. 10.1109/ICECS58634.2023.10382858 . cea-04455302

**HAL Id: cea-04455302**

**<https://cea.hal.science/cea-04455302>**

Submitted on 13 Feb 2024

**HAL** is a multi-disciplinary open access archive for the deposit and dissemination of scientific research documents, whether they are published or not. The documents may come from teaching and research institutions in France or abroad, or from public or private research centers.

L'archive ouverte pluridisciplinaire **HAL**, est destinée au dépôt et à la diffusion de documents scientifiques de niveau recherche, publiés ou non, émanant des établissements d'enseignement et de recherche français ou étrangers, des laboratoires publics ou privés.

# A wide-spectrum 550-1600 nm, 16k VIS + 8 NIR pixels, high-dynamic range image-sensor for biomedical applications

Laurent Alacoque  
DOPT Department  
Univ. Grenoble Alpes, CEA, Leti  
Grenoble, France  
laurent.alacoque@cea.fr

David Coriat  
DSCIN Department  
Univ. Grenoble Alpes, CEA, List  
Grenoble, France  
david.coriat@cea.fr

Jean-Michel Tualle  
LPL, UMR 7538  
Université Sorbonne Paris-Nord  
Villetaneuse, France  
tualle@univ-paris13.fr

Valentin Espinas  
Aix Marseille Univ, CNRS, Centrale  
Marseille, Institut Fresnel  
Aix Marseille University, CERIMED  
Marseille, France  
valentin.espinas@fresnel.fr

Xavier Alacoque  
Anesthesia, intensive care  
Oncopole Claudius Regaud  
Toulouse, France  
alacoque.xavier@iuct-oncopole.fr

Anabela Da Silva  
Aix Marseille Univ, CNRS, Centrale  
Marseille, Institut Fresnel  
Aix Marseille University, CERIMED  
Marseille, France  
anabela.dasilva@fresnel.fr

**Abstract**— This paper presents an Application-Specific Integrated Circuit (ASIC) wide-spectrum image sensor and its sensing-module and system. It is made of an integrated visible image sensor, an external NIR-SWIR photodiodes acquisition system and on-chip Analogue to Digital conversion and provides a digital interface to a portable, fully integrated host system based on a raspberry-pi with a dedicated “hat” board. The system is capable of real-time Diffuse Optical Imaging in a wide spectrum with a resolution of 3x16k visible images and 3x8 NIR photodiodes. A signal-to-noise ratio of 66dB in the NIR domain was attained at a total power of 18.4 mW.

**Keywords**—biomedical sensor; diffuse optical imaging; diffuse optical spectroscopy; image sensor; NIR; SWIR.

## I. INTRODUCTION

Innovations in wearable devices for tele-home healthcare (tele-medicine) can enhance usability, efficiency, and popularity of home-based telemedicine. These devices not only allow long-term, continuous, and unobstructed monitoring of physiologic information, such as heart rate (HR), blood pressure (BP), blood oxygen saturation (SaO<sub>2</sub>), and respiration, but can also provide more realistic indications of the patient’s health status, and information that is otherwise inaccessible in clinical settings. Optical diagnosis with diffuse light is a promising method for compact and low-cost non-invasive monitoring. The simplest configuration for a wearable device is certainly the reflectance geometry, where the sources and sensors are placed on the same side of the medium (Fig. 1): this geometry is relevant for thick tissue like the forearm or the ankle.

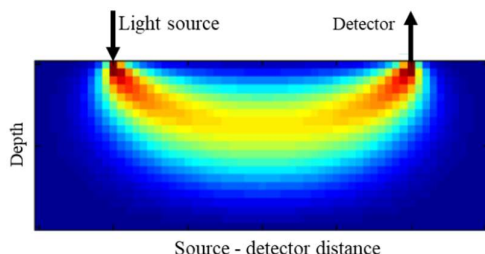


Fig. 1 Light-path density between source and detector in a scattered media.

Diffuse Optical Spectroscopy (DOS) is now a broadly used method to perform the dosimetry of various physiological parameters through spatially distributed non-invasive measurements of light backscattered from a tissue or

organ [1,2]. Additionally, if a spatially-resolved sensor is used, inversion protocols provide the ability to specifically target the properties of a specific zone of the tissue, like a vein for instance. Although very popular for oximetry, by tuning the wavelengths, one can potentially have access to the quantification of other parameters (lipids, collagen, ketones, ...) provided that the spectral response of the sensor is wide enough and extends into the Short-Wave Infrared (SWIR) domain. However, the light flux decreases exponentially with the distance from the source, and the implementation of such protocols requires accurate measurements with a high-dynamic range (HDR). Therefore, a HDR, wide-spectrum sensor with spatial resolution is needed to achieve localized DOS for a wide range of physiological parameters dosimetry.

## II. DUAL-SPECTRUM IMAGE SENSOR

We designed a dual-spectrum image sensor ASIC using Tower Semiconductors CMOS 180nm technology with Camera Integrated System (CIS) extensions using a thicker epitaxy of 18 $\mu$ m to improve Quantum Efficiency in the NIR domain.

### A. Overview

Fig. 2 presents the circuit overview along with its annotated layout. The 5 x 5 mm<sup>2</sup> circuit is made out of a 4.35 x 2.3 mm<sup>2</sup> visible-photodiode array along with an 8-channels high dynamic range Capacitive Trans-Impedance Amplifier (CTIA) that provides measurement capability for eight external 1.3 x 0.8 mm<sup>2</sup> InGaAs NIR-SWIR 300  $\mu$ m diameter PIN photodiodes [3]. Column-parallel Analogue-to-Digital Conversion (ADC) is responsible for the digitization of internal pixels as well as the conversion of the NIR-SWIR residual outputs, thus allowing for consistent photometric results between visible and NIR-SWIR subsystems. A digital core provides Finite-State Machines (FSM) for the acquisition processes and exposes the circuit’s functionalities to the host using control, configuration and results registers accessible through a single SPI slave bus and a minimal Command-Address-Data protocol.

We kept the circuit’s Inputs/Outputs (IO) count to a minimum in order to limit wire bonding to a single-sided bond-pad row at the bottom. This allows for the abutment of several circuits in the horizontal direction as well as reducing the distance between the pixel array and the top edge of the pixel array.

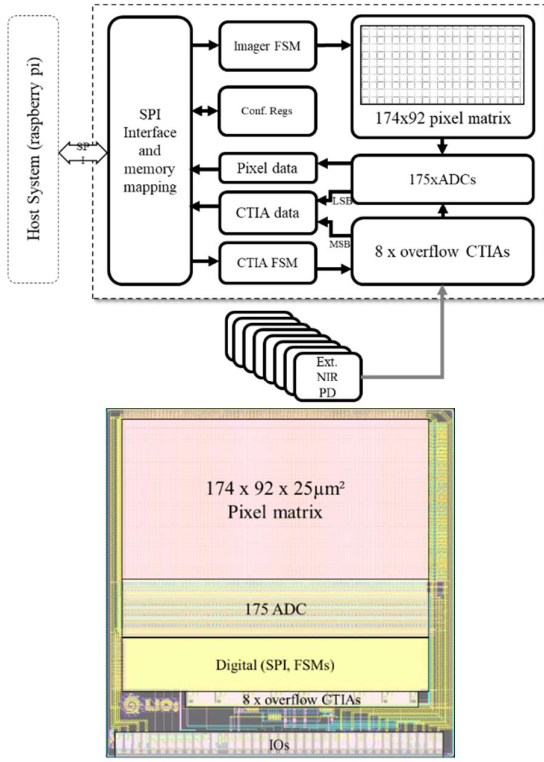


Fig. 2 System overview (top) and annotated layout (bottom) of the ASIC.

### B. Embedded visible image sensor

The embedded visible image sensor consists of an array of 174 by 92,  $25 \times 25 \mu\text{m}^2$ , 5T pinned-photodiodes provided by TowerSemiconductors. The largest photodiodes were selected in order to provide a greater response for low-photon-count operations (low light, or large absorption by the middle).

#### 1) Pixel readout

Fig. 3 presents the schematic of the pixel. Before integration, the PIN photodiode is reset to VDD either using the global SNAP signal in snapshot mode or through the line-wise RST/TX combination in rolling-shutter mode. To read the pixel value, the RST signal is used to reset the sense-node and the SEL isolation transistor connects the source-follower transistor to the shared column, thus establishing the reset voltage to the bus where the black level can be sampled. The TX signal is then triggered, transferring the photodiode's accumulated charge to the sense-node and establishing the signal to the bus where it can be converted to digital.

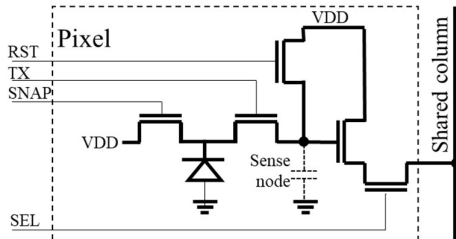


Fig. 3 Pixel schematic for the 5T photodiode.

Fig. 4 presents the end-of-column circuit. At the bottom of the column, a current-source transistor completes the pixel's source-follower. A sample and hold circuit allows the sampling of black and signal levels. An analog multiplexer provides an alternate input to the ADC for the CTIA residue

of NIR-SWIR acquisition operation (see section II.C). The end-of-column circuit is completed by a Delta-Sigma modulator coupled to a digital integrator that provide analogue to digital conversion for the pixel value.

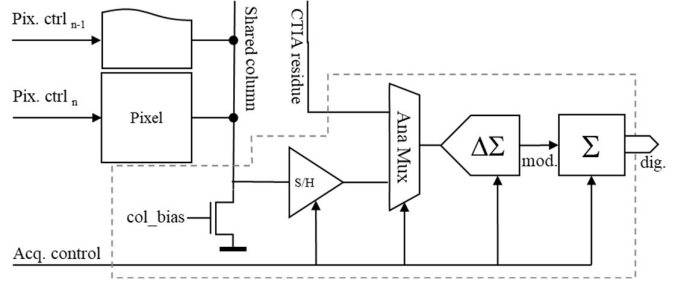


Fig. 4 End-of-column schematic

#### 2) Analog to digital conversion

In order to guarantee a high linearity in the pixel response, we designed a column-wise  $25 \mu\text{m}$ -wide 3rd order feed-forward Incremental Delta-Sigma ADC depicted on Fig. 5. System-level simulations using Matlab were performed to determine the attenuation and feed-forward coefficients in order to guarantee a high stability while preserving the smallest over-sampling ratio for conversion speed. With the coefficients shown on Fig. 5, Delta-Sigma modulation stability was achieved over the pixel voltage swing and a resolution of 13 bits is attained with an OSR of 130 while accounting for a 3.5% variability of integration coefficients due to capacitor mismatch. Finally, a digital filter implementing a third-order digital integrator is responsible for the digital filtering of modulation [4].

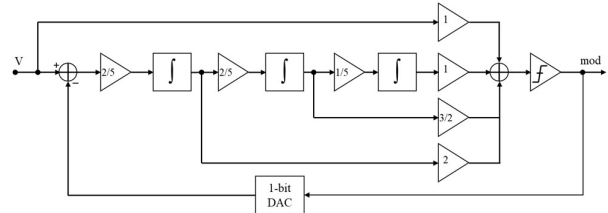


Fig. 5 Overview of the Feed-Forward 3rd Order Delta-Sigma Modulator

The Delta-Sigma modulator is implemented using switched capacitors circuits. Unit capacitor of 150 fF was chosen to achieve the best tradeoff between thermal noise, surface and power for the desired resolution.

#### 3) Imager control

The host starts visible image acquisition by setting the VIS\_ACQ bit in the control register through SPI. This starts the image sensor FSM that orchestrates control signals for the exposure time, readout and pixel A-D conversion. Once a full line is converted in parallel, the digital pixels are stored in 174 16b pixel registers mapped onto the SPI-addressable memory and the End Of Conversion (EOC) bit is set in the circuit's state register. The host is responsible for polling this register and to retrieve pixel data as soon as they are available. Once the pixels data are read, the host clears the EOC bit to start the readout and A-D conversion of the next line.

### C. NIR Photodiodes acquisition

Additionally to the visible light, the circuit is capable of measuring the charges generated by eight external NIR-SWIR photodiodes. To account for the great variation caused by the absorption windows in water, the charge to voltage conversion

is performed using a multi-gain CTIA with overflow capability [5,6]. The architecture is presented on Fig. 6.

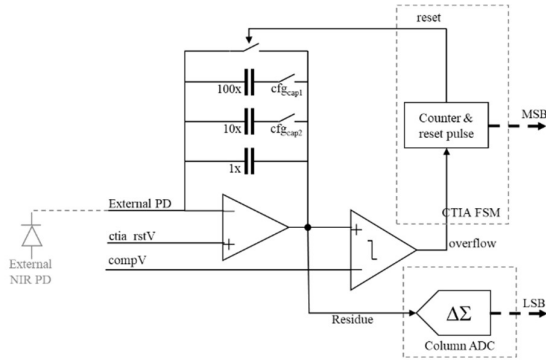


Fig. 6 External NIR Photodiodes acquisition subsystem.

On this figure, an external NIR photodiode cathode is connected to the multi-gain CTIA (left). The capacitor bank is made out of a unit capacitor of 150 fF and two switchable arrangements of 10 and 100 unit capacitors whose switches are controlled by bits from the configuration register. During idle operations, the integration capacitors are short-circuited and the external\_pd pin is therefore maintained to the ctia\_rstV voltage through the feedback loop of the operational trans-amplifier (OTA).

To start the acquisition, the host sets the NIR\_ACQ bit in the control register that causes the reset to be released, starting the integration phase. During integration, charges are drawn by the external photodiode at the rate of photon absorption thus forcing the OTA to provide the same amount of charge to the opposing plate of the capacitor to maintain a constant voltage on external\_pd pin. This results in the OTA’s output to raise, hence providing charge-to-voltage conversion. When the photon rate is important or in case of long integration times, the CTIA’s output increases and could saturate at the circuit power voltage. To prevent this, when the output raises above the threshold voltage compV, the comparator triggers, which starts a digital FSM that increments an overflow count register and performs an analogue reset cycle of the CTIA, thus restoring its output voltage to ctia\_rstV and a new cycle begins.

When the desired integration time is reached, the host clears the NIR\_ACQ bit. This event triggers the sampling of the eight CTIA residual voltages along with the voltages of ctia\_rstV and compV. Those 10 voltages are converted to 16b digital words using 10 of the 174 column ADCs, forming the LSB part of the external photodiodes signal acquisition. The results are then stored into SPI-mapped 16b registers alongside their respective 16b overflow counters which are available for the host system to retrieve. The full-range value of the acquired NIR signal is computed on the host using respective LSB and MSB values along with the digitized value of (compV – ctia\_resetV) which amounts to the magnitude of one MSB in LSB unit.

Based on the magnitude of the eight MSB values, the host is responsible for configuring the 10x and 100x gains in order to achieve the best acquisition Signal-to-Noise Ratio (SNR) for each one of the external photodiodes.

### III. SYSTEM INTEGRATION

We designed a 35 x 22mm<sup>2</sup> sensing module made out of 3 circuits and 24 external NIR photodiodes. This module allows

to carefully align the NIR photodiodes and image sensors in a compact form and provides a high-density connector for cable connection.

In this configuration, the spatial arrangement of the circuit and external photodiodes were chosen so that a wrist-handled module sensing elements would naturally cross the wrist veins where blood parameters measurements are targeted, hence facilitating inversion methods and improving VIS/NIR spatial correlation.

The module is embedded into a wearable 3D-printed case along with Fiber-optics Plate optics and a wrist-band for easy operation. It is connected to a specially-designed raspberry pi “hat” board that provides all the necessary power domains, polarization and control using the pi’s embedded SPI-master and clock generator. A firmware and a graphical user-interface were designed to facilitate the module operation. Fig. 7 shows the different elements of the system.

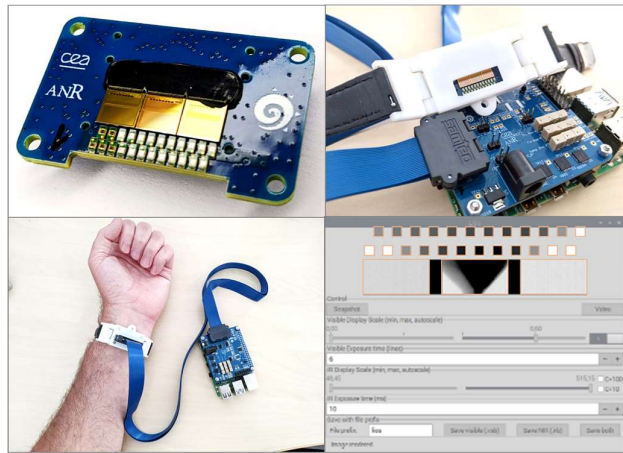


Fig. 7 Top left: Sensing module (3 circuits + 24 photodiodes), top right: module enclosed in a wristband case connected to the raspberry-pi host, bottom left: typical utilisation of the system, bottom right: graphical user interface running on the raspberry showing the acquisition of a contact image of the corner of a business card. The image is made out of NIR-SWIR photodiodes (24 top squares) and the visible image sensors (3 rectangles).

## IV. RESULTS

### A. Normalized responsivity of the module

Fig. 8 shows the theoretical normalized responsivity of the module extrapolated from the providers’ datasheets (dashed) along with our own measurements in the visible domain (black). Due to limitations of our light source, only the visible spectrum was measured. We explain the lower measured responsivity in the [500 nm – 550 nm] wavelengths range by the augmented reflectance of silicon in this range.

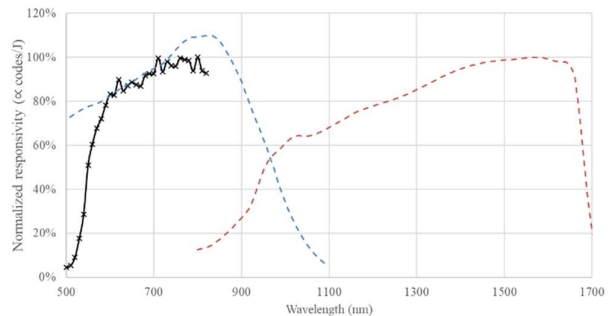


Fig. 8 Theoretical normalized responsivity of the system (dashed) and experimental results in the visible domain (solid).

## B. Visible imaging results

Fig. 9 shows some image results from the visible subsystem where dashed areas account for the physical distance between pixel matrices. The top image shows the measurement of pixel photo-response uniformity acquired using an integrating sphere. A maximum photo-response non-uniformity of 1.8% was obtained without optics and 3% when using Fiber-Optics Plate. The bottom image shows the picture of a translucent ruler graduated in millimeters obtained by direct contact on the image sensors.

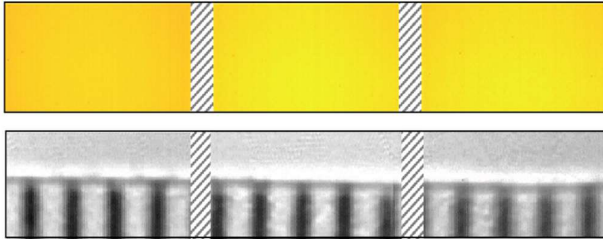


Fig. 9 Image of an integrating sphere for photoresponse uniformity (top) and contact-image of a translucent ruler (bottom).

## C. NIR-SWIR imaging results

Fig. 10 and Fig. 11 show the results for NIR-SWIR photodiodes acquisition at 780 nm. To account for the recommended absorption dose for human, we limited the irradiance of the source to  $150 \text{ nW/cm}^2$  and a maximum integration time of 1 s. Fig. 10 presents the raw signal acquisition (top) and the affine-corrected responses (bottom). Each point represents a single acquisition without averaging. The residual error after fitting is plotted on Fig. 11 (top) along with the SNR (bottom). A SNR of 66dB is attained for irradiance greater than  $40 \text{ nW/cm}^2$ . The dashed line represents a 10 dB/decade trend.

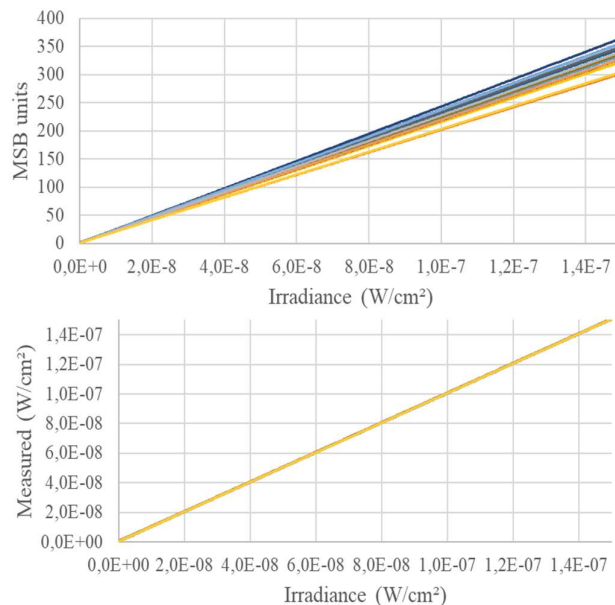


Fig. 10 Raw responses (top) and superimposed responses after affine correction (bottom) for NIR photodiodes at 780 nm

## D. Power consumption

Measured power consumption for the acquisition module ranges from 4.8 mW in standby mode to 18.4 mW in full-speed VIS + NIR-SWIR acquisition.

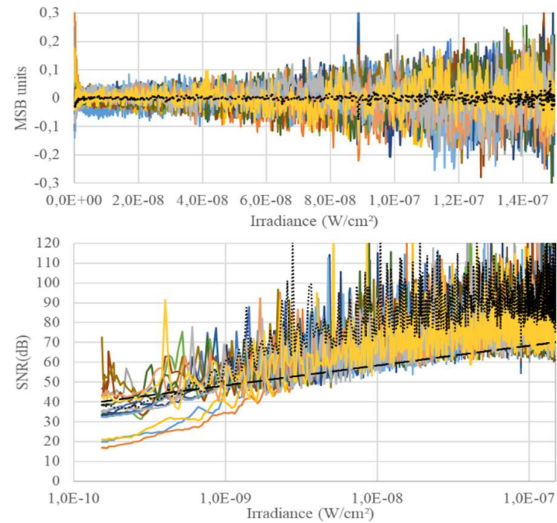


Fig. 11 Residual error (top) and signal-to-noise ratio (bottom) after affine correction for the external NIR photodiodes at 780 nm (dotted black points represent the median error and SNR among all photodiodes of the module).

## V. CONCLUSION

A spatially-resolved, VIS-NIR-SWIR dual-spectrum image sensor was presented. It can acquire images in the 550-1600 nm wavelength range thus enabling a variety of biomedical applications by performing localized DOS over a wide spectral range. With a compact form factor of only  $35 \times 22 \text{ mm}^2$ , the sensing module is embedded in a wristband coupled to a simple raspberry-pi host. The module can acquire 48 kpix, 13b visible images on a  $2.3 \times 15 \text{ mm}^2$  area along with 24 NIR-SWIR photodiodes. This resolution allows to target specific spatial regions thank to inversion protocols. A raw signal-to-noise ratio of 66 dB was attained for the NIR photodiodes at a power of 18.4 mW in full operation mode.

## ACKNOWLEDGMENT

Authors wish to thank the French National Research Agency (ANR) for the funding of this project referenced as ANR-16-CE19-0012.

## REFERENCES

- [1] T. Vo-Dinh, "Biomedical Photonics Handbook ,Therapeutics and Advanced Biophotonics (1st ed.)", Chap. 4, Boca Raton: CRC Press, 2003. doi: 10.1201/b17288
- [2] M. Romine, A. Moazzen, L. Luong, K. Cho and S. Y. Lee, "Portable Diffuse Reflectance Spectroscopy for Non-Invasive and Quantitative Assessment of the Parathyroid Glands Viability", in *2023 IEEE International Opportunity Research Scholars Symposium (ORSS)*, Atlanta, GA, USA, 2023, doi: 10.1109/ORSS58323.2023.10161759
- [3] Hamamatsu-photonics, "InGaAs PIN Photodiode G13176-003P," [Online]. Available: [https://www.hamamatsu.com/g13176\\_series\\_kird1131e.pdf](https://www.hamamatsu.com/g13176_series_kird1131e.pdf). [Accessed 2023]
- [4] J. Markus, J. Silva and G. C. Temes, "Theory and applications of incremental Delta-Sigma converters", *IEEE Transactions on Circuits and Systems I: Regular Papers*, vol. 51, no. 4, pp. 678-690, 2004. doi: 10.1109/TCSI.2004.826202.
- [5] F. Guellec, A. Peizerat, M. Tchagaspanian, E. De Borniol, S. Bisotto, L. et al., "A 25 $\mu\text{m}$  pitch LWIR focal plane array with pixel-level 15-bit ADC providing high well capacity and targeting 2mK NETD" in *Proc. SPIE 7660, Infrared Technology and Applications XXXVI*, 2010. doi: <https://doi.org/10.1117/12.849684>
- [6] A. Peizerat, M. Arques, P. Villard, J.-L. Martin and G. Bouvier, "Pixel-level ADC by small charge quantum counting", in *13th IEEE International Conference on Electronics, Circuits and Systems*, 2006. doi: 10.1109/ICECS.2006.379815.